Supporting Information for "Similar millennial climate variability on the Iberian margin during two early Pleistocene glacials and MIS 3"

B. Birner[1], D. A. Hodell[1], P. C. Tzedakis[2], L. C. Skinner [1]

[1]Godwin Laboratory for Palaeoclimate Research, Department of Earth Sciences, University of Cambridge, Cambridge, United Kingdom.

[2]UCL Department of Geography, University College London, London, United Kingdom.

Corresponding author: B. Birner, Godwin Laboratory for Palaeoclimate Research, Department of Earth Sciences, University of Cambridge, Cambridge, United Kingdom

Now at Scripps Institute of Oceanography, University of California San Diego, La Jolla, California 92037, USA. (bbirner@ucsd.edu)

Contents of this file

Introduction

In this supplement, we provide further explanation for the methods and analysis presented in the text, including:

1. How our modified age model was constructed and how it compares to age models of *Hodell et al.* [2015] (Fig. S1).

2. How $\delta^{18}O_w$ was calculated using Mg/Ca paleothermometry (Text S1) and how we estimated the propagated error on both proxy records (Text S2).

3. How the records were detrended and cross-correlation analysis applied to estimate the phase relationship among proxy variables at Site U1385 (Text S3). We performed the cross-correlation analysis in time and depth domains (Text S4 and Fig. S2).

4. How the record from Site U1385 was correlated to Site U1308 and Site 983 in order to compare the isotope data at Site U1385 with the IRD proxies at higher latitude sites in the North Atlantic (Figs. S3 & S4 and Tables S1 & S2). The Site 983 and Site U1308 benthic $\delta^{18}O$ and IRD records are shown on their respective age models in Figure S5.

5. In Figure S6, the wavelet and REDFIT [*Schulz*, 2002] time series analysis of the Site U1385 isotope record were repeated using the insolation tuned age model of *Hodell et al.* [2015].

6. Lastly, the millennial-scale variability observed in the stable isotope records of Site U1385 are compared with elemental variations in sediment composition measured by core scanning XRF at the same site [*Hodell et al.*, 2015] (Text S5 and Fig. S7).

Text S1. Mg/Ca Temperature Calibration and δ^{18}O$_w$ Calculation

Deep water temperatures and seawater oxygen-isotope compositions were obtained following the methodology of *Elderfield et al.* [2012]. Mg/Ca temperatures were calculated using the relationship

$$Mg/Ca = 1.0 + 0.1\,(T°C) \quad (1)$$

based on the *Elderfield et al.* [2010] core top calibration for *Uvigerina spp.*. *Elderfield et al.* [2012] combined Equation 1 with the oxygen-isotope paleothermometry equation of *Shackleton* [1974] to obtain the δ^{18}O$_w$ relationship

$$\delta^{18}O_w = \left(\delta^{18}O_{calcite} + 0.27\right) - 0.25\left(16.9 - \frac{\frac{Mg}{Ca} - 1}{0.1}\right) \quad (2)$$

where δ^{18}O$_w$ is reported relative to Standard Mean Ocean Water (SMOW).

Text S2. Data Quality and Error Progression

The sensitivity of Mg/Ca to deep water temperature in the foraminifera species *Uvigerina* is a matter of ongoing debate, but calculated deep water temperatures are only moderately dependent on the exact numerical representation of this sensitivity. *Elderfield et al.* [2010] reported a standard error of ±0.013 mmol/mol/C for their calibration. Assuming an analytical error of <6% for Mg/Ca measurements of foraminiferal calcite, this yields a standard error of less than ±0.87°C for temperatures in the study range (<5°C). The standard error increases with temperature and for temperatures lower than 3°C, the standard error is less than ±0.65°C. Precision of repeated oxygen-isotope measurements on laboratory standards was ±0.08‰. The uncertainty of repeated measurements of real samples is likely higher but has not been quantified. For the purpose of error propagation, an uncertainty of ±0.08‰ is thus assumed. No uncertainty evaluation was offered by

Shackleton [1974] for his oxygen-isotope paleothermometry calibration. After propagating errors associated with the Mg/Ca and oxygen-isotope measurements as well as the uncertainties of Mg/Ca paleothermometry, a standard error of less than ±0.23‰ is estimated for $\delta^{18}O_w$. An additional significant error is probably associated with the oxygen-isotope paleothermometry calibration but could not be quantified for this calculation.

Text S3. Time Series Detrending and Cross-correlation

Time series were 'detrended' for wavelet and cross-correlation analysis. The data sets were interpolated to equal time steps of 0.2 ka and smoothed independently with two Gaussian kernels of 0.6-ka and 10-ka width (i.e., the long-term trend), respectively. The long-term trend was subtracted from the (0.6-ka) presmoothed data to emphasize the millennial-scale variability in the detrended residual.

The cross-correlation of two time series indicates the degree of similarity as a function of the assumed (time) lag between both series. Peaks in the correlation coefficient r reveal the offsets that yield the best agreement between the two time series. The sign of r indicates whether the lagged proxies are in-phase or anti-phased. Assuming that the best agreement between the detrended proxy time series is achieved when the isotope excursions associated with millennial events are aligned, cross-correlating planktonic δ^{18}O and benthic δ^{18}O (or benthic δ^{13}C) is used to evaluate the relative phasing between the proxies. Several (secondary) maxima of correlation may occur since further increasing the offset will eventually lead to alignments with the next millennial event due to their semi-periodic nature. Thus we interpret the highest cross-correlation peak to reflect the closest estimate of the true lag between proxies. The stratigraphic pattern interpreted to reflect the bipolar see-saw at the Iberian margin during MIS 3 is characterized by a lead of planktonic δ^{18}O over benthic δ^{18}O, whereas planktonic δ^{18}O is anti-phased to benthic δ^{13}C with nearly no apparent lag [*Shackleton et al.*, 2000, 2004; *Skinner et al.*, 2007].

Text S4. U1385 Cross-Correlation in Depth Domain

The cross-correlation procedure for the Site U1385 isotope records was also carried out in depth domain at 2 cm ($\approx$ 200 a) resolution to evaluate age model influences. Figure S2 shows that planktonic δ^{18}O lags benthic δ^{18}O by 8 cm and leads benthic δ^{13}C by $<$2 cm. Assuming sedimentation rates of $\sim$10 cm/ka, these depth-lags are in good agreement with the time domain results of 600 a and $<$200 a, respectively.

Text S5. Sediment Element Ratios

Hodell et al. [2013] suggested that the elemental composition of Iberian margin sediment reflects changes in the relative proportion of two sources, biogenic or detrital material. Ca and Sr are primarily of biogenic origin whereas Ti and Zr are mostly derived from continental detritus. For the last glacial period, Ca/Ti resembles the Greenland ice core δ^{18}O record in great detail, capturing most of the Dansgaard-Oeschger events [*Hodell et al.*, 2013]. Thus, Ca/Ti may serve as an additional proxy of millennial-scale variability.

Similar to MIS 3, Ca/Ti closely follows planktonic δ^{18}O during MIS 38 (and MIS 40, not shown) in Figure S7. Zr/Sr is the mirror image of Ca/Ti and peaks during stadials in MIS 38 (and MIS 40). *Hodell et al.* [2013] attributed changes in Ca/Ti and Zr/Sr on millennial time scales to variability in the deposition of biogenic material, due to higher biological productivity during interstadials compared to stadials. The comparable agreement between Ca/Ti and planktonic δ^{18}O during MIS 3 and MIS 38 suggests that this process also operated in the late early Pleistocene. Moreover, the results support the use of XRF data as a proxy for abrupt climate change in the 41-ka world [*Hodell et al.*, 2015].

References

Barker, S., G. Knorr, R. Edwards, and F. Parrenin (2011), 800,000 years of abrupt climate variability, *Science*, *334*, 347–352, doi:10.1126/science.1203580.

Elderfield, H., M. Greaves, S. Barker, I. R. Hall, A. Tripati, P. Ferretti, S. J. Crowhurst, L. Booth, and C. Daunt (2010), A record of bottom water temperature and seawater $\delta^{18}O$ for the Southern Ocean over the past 440 kyr based on Mg/Ca of benthic foraminiferal Uvigerina spp., *Quaternary Science Reviews*, *29*(1–2), 160–169, doi:10.1016/j.quascirev.2009.07.013.

Elderfield, H., P. Ferretti, S. J. Crowhurst, I. N. Mccave, D. A. Hodell, and A. M. Piotrowski (2012), Evolution of ocean temperature and ice volume through the Mid-Pleistocene climate transition, *Science*, *337*, 704–710, doi:10.1126/science.1221294.

Hodell, D. A., J. E. T. Channell, J. H. Curtis, O. E. Romero, and U. Röhl (2008), Onset of "Hudson Strait" Heinrich events in the eastern North Atlantic at the end of the middle Pleistocene transition (∼640 ka)?, *Paleoceanography*, *23*, PA4218, doi:10.1029/2008PA001591.

Hodell, D. A., S. J. Crowhurst, L. Skinner, P. C. Tzedakis, V. Margari, J. E. T. Channell, G. Kamenov, S. Maclachlan, and G. Rothwell (2013), Response of Iberian Margin sediments to orbital and suborbital forcing over the past 420 ka, *Paleoceanography*, *28*, 185–199, doi:10.1002/palo.20017.

Hodell, D. A., L. Lourens, S. J. Crowhurst, T. Konijnendijk, R. Tjallingii, F. Jimenez-Espejo, L. C. Skinner, P. C. Tzedakis, and Members of the Shackleton Site Project (2015), A reference time scale for Site U1385 (Shackleton Site) on the Iberian Margin, *Global Planetary Change*, *133*, 49–64, doi:10.1016/j.gloplacha.2015.07.002.

Konijnendijk, T. Y. M., M. Ziegler, and L. J. Lourens (2014), Chronological constraints on Pleistocene sapropel depositions from high-resolution geochemical records of ODP Sites 967 and 968, *Newsletters on Stratigraphy*, *47*(3), 263–282, doi:10.1127/0078-0421/2014/0047.

Laskar, J., P. Robutel, F. Joutel, M. Gastineau, A. C. M. Correia, and B. Levrard (2004), A long-term numerical solution for the insolation quantities of the Earth, *Astronomy and Astrophysics*, *428*, 261–285, doi:10.1051/0004-6361:20041335.

Paillard, D., L. Labeyrie, and P. Yiou (1996), Macintosh Program performs time-series analysis, *Eos, Trans. AGU*, *77*(39), 379, doi:10.1029/96EO00259.

Raymo, M., K. Ganley, S. Carter, D. Oppo, and J. McManus (1998), Millennial-scale climate instability during the early Pleistocene epoch, *Nature*, *542*, 699–702, doi:10.1038/33658.

Schulz, M. (2002), On the 1470-year pacing of Dansgaard-Oeschger warm events, *Paleoceanography*, *17*(2), 1–9, doi:10.1029/2000PA000571.

Shackleton, N. J. (1974), Attainment of isotopic equilibrium between ocean water and the benthonic foraminifera genus Uvigerina: Isotopic changes in the ocean during the last glacial, in *Les Méthodes Quantitatives D'Etude des Variations du Climat au cours du Pléistocène*, vol. 219, pp. 203–210, Colloque international du CRNS, Gif-sur-Yvette.

Shackleton, N. J., M. A. Hall, and E. Vincent (2000), Phase relationships between millennial-scale events 64,000-24,000 years, *Paleoceanography*, *15*(6), 565–569, doi: 10.1029/2000PA000513.

Shackleton, N. J., R. G. Fairbanks, T. Chiu, and F. Parrenin (2004), Absolute calibration of the Greenland time scale: implications for Antarctic time scales and for Δ^{14}C, *Quaternary Science Reviews*, *23*(14–15), 1513–1522, doi: 10.1016/j.quascirev.2004.03.006.

Skinner, L. C., H. Elderfield, and M. A. Hall (2007), Phasing of millennial climate events and Northeast Atlantic deep-water temperature change since 50 ka BP, in *Ocean Circulation: Mechanisms and Impacts - Past and Future Changes of Meridional Overturning, Geophys. Monogr. Ser., vol 173*, edited by A. Schmittner, J. C. H. Chiang, and S. R. Hemming, pp. 197–208, AGU, Washington, D. C., doi:10.1029/173GM14.

Vautravers, M. J., and N. J. Shackleton (2006), Centennial-scale surface hydrology off Portugal during marine isotope stage 3: Insights from planktonic foraminiferal fauna variability, *Paleoceanography*, *21*, PA3004, doi:10.1029/2005PA001144.

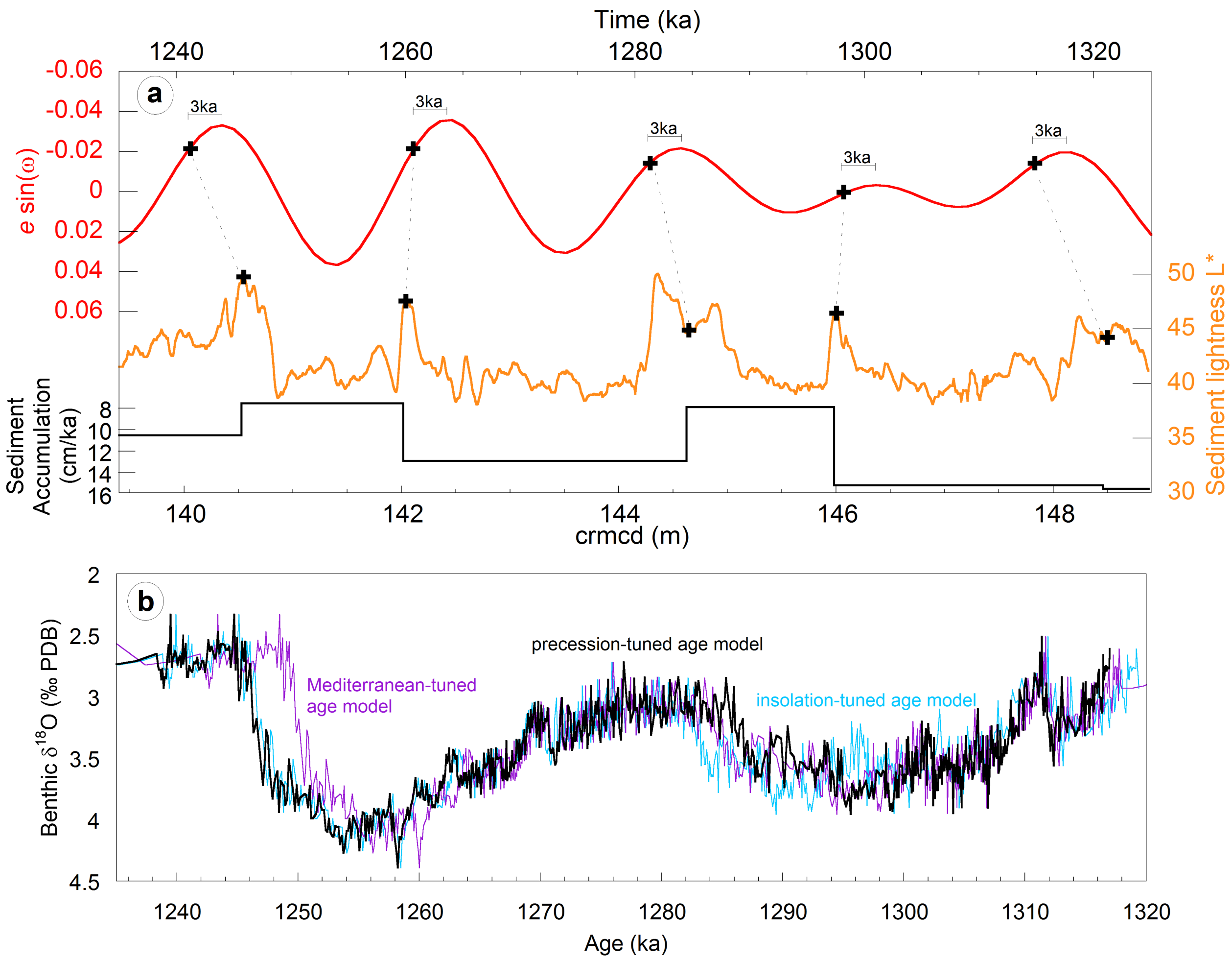

Figure S1. (a) Tie points for tuning between the U1385 sediment lightness indicator L* on the corrected revised meter composite (crmcd) depth and the precession parameter [*Laskar et al.*, 2004]. The sediment accumulation rates deduced from the tuning process are shown for reference. (b) The U1385 benthic $\delta^{18}O$ record on the modified tuned age model of this study is compared to the same record plotted on two different age models of *Hodell et al.* [2015] that were obtained by tuning to local summer insolation and the Mediterranean sapropel cyclostratigraphy of *Konijnendijk et al.* [2014], respectively.

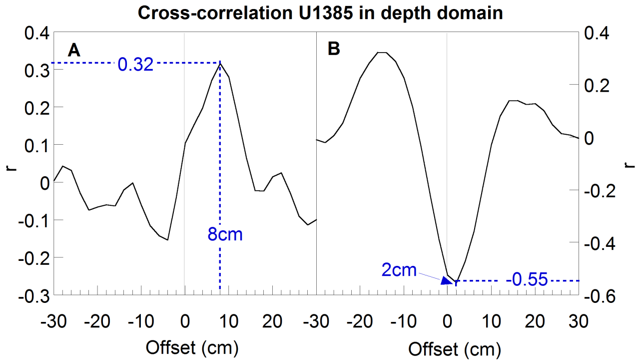

Figure S2. Cross-correlation of Site U1385 in depth domain. (A) Cross-correlation of benthic $\delta^{18}O$ and planktonic $\delta^{18}O$. (B) Cross-correlation of planktonic $\delta^{18}O$ and benthic $\delta^{13}C$. Positive offset on the x-axis denote a lead of benthic $\delta^{18}O$ in (A) or planktonic $\delta^{18}O$ in (B), respectively. The original data was resampled to 2-cm resolution and smoothed with a 6-cm Gaussian kernel. The smoothed series were detrended by subtracting a 100-cm Gaussian filter. The cross-correlation of the residuals was calculated in Analyseries [*Paillard et al.*, 1996].

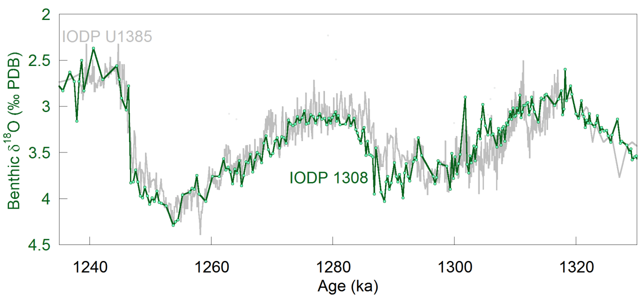

Figure S3. Benthic $\delta^{18}O$ records of Sites U1308 [*Hodell et al.*, 2008] and U1385 on the precession-tuned age model of this study. The time series were correlated by optically comparing the benthic $\delta^{18}O$ records.

Table S1. IODP U1385 and U1308 Age-Depth Tie Points

IODP U1308 depth (m)	IODP U1385 modified tuned age (ka)
89.50	1246.60
90.07	1257.62
91.25	1279.35
92.91	1302.35
93.35	1307.00
94.45	1319.12

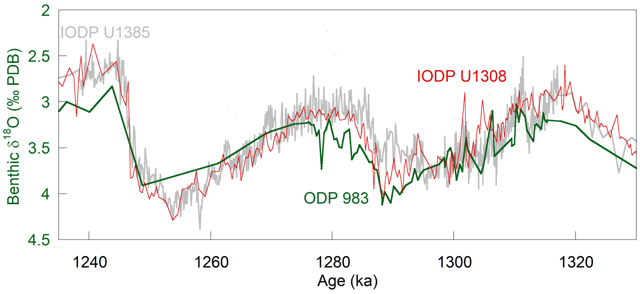

Figure S4. Benthic δ^{18}O records of Sites 983 [*Raymo et al.*, 1998] and U1385 on the precession-tuned age model of this study. The time series were correlated by optically comparing the benthic δ^{18}O records. For the ambiguous correlation during the termination 39/40 benthic δ^{18}O from IODP Site U1308 was used to confirm the age model.

Table S2. IODP U1385 and ODP 983 Age-Depth Tie Points

ODP 983 depth (m)	**IODP U1385 precession-tuned age (ka)**
157.46	1246.27
162.56	1288.60
163.91	1302.00
165.25	1311.69
166.40	1317.85

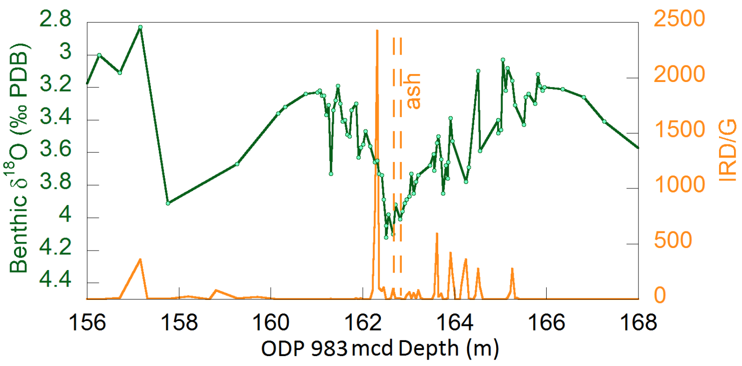

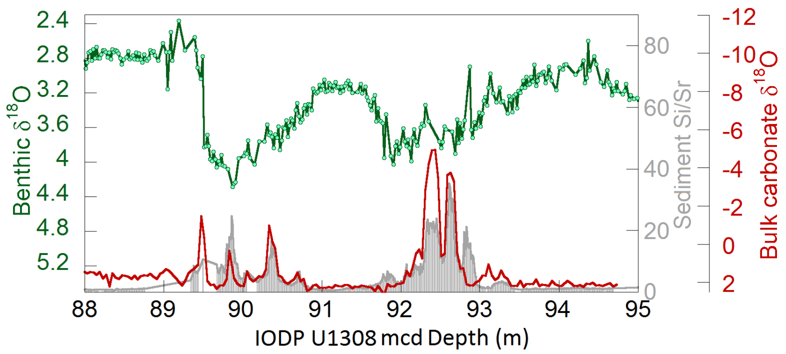

Figure S5. IRD proxy and benthic δ^{18}O records from (a) ODP Site 983 [*Raymo et al.*, 1998] and (b) IODP Site U1308 [*Hodell et al.*, 2008] on their respective depth scales. Two prominent ice-rafting events were detected at Site U1308 during termination 37/38 coinciding with two major δ^{18}O decreases. The Site 983 IRD record for the same interval also indicates ice-rafting but is only available at low resolution. In contrast, no ice-rafting event is detected at Site U1308 during the termination 39/40, while one IRD peak occurs ∼20 cm (≈ 2 ka) after the beginning of the deglacial δ^{18}O decrease at Site 983.

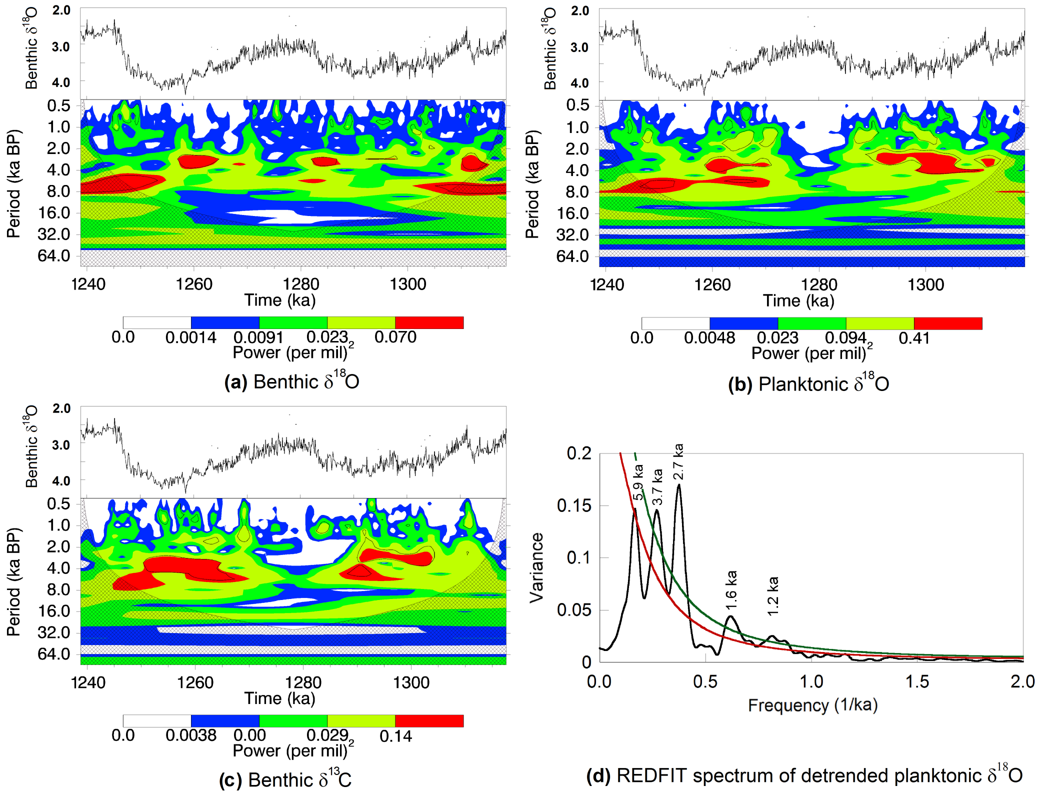

Figure S6. Time series analysis of the detrended U1385 isotope records as presented in Figure 4 of the text but for the insolation-tuned age model of *Hodell et al.* [2015].

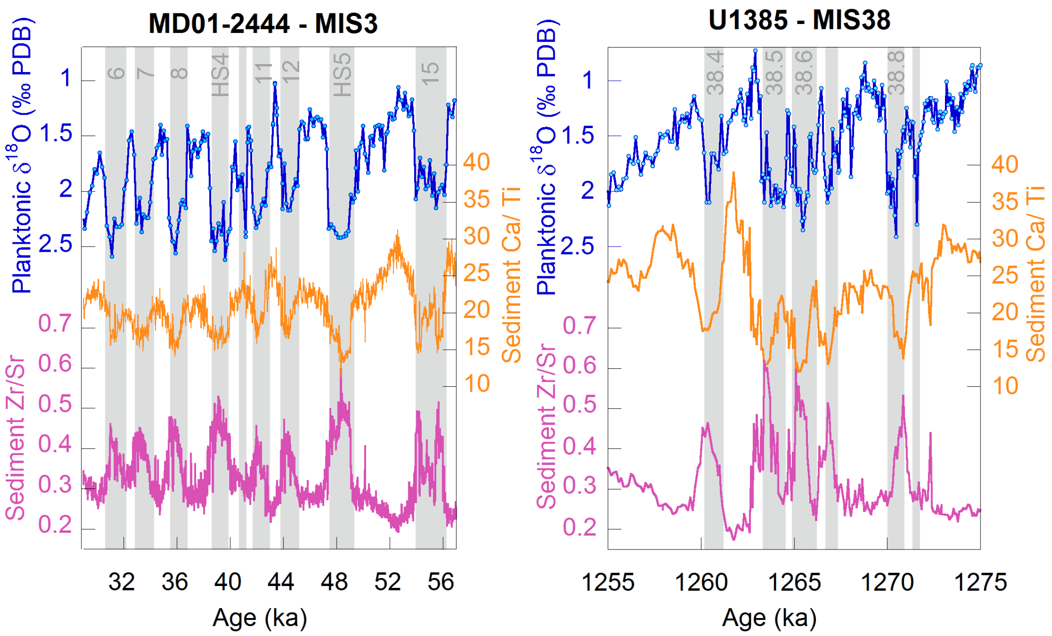

Figure S7. Comparison of planktonic δ^{18}O and sediment elemental ratios Zr/Sr and Ca/Ti during MIS 38 (right) and MIS 3 (left) [*Hodell et al.*, 2015]. Both elemental ratios indicate changes in the relative proportion of biogenic and detrital sediment. MD01-2444 data [*Hodell et al.*, 2013; *Vautravers and Shackleton*, 2006] are shown on the 'Greenland Synthetic' time scale of *Barker et al.* [2011].